Pergamon

PII: S0301-9322(96)00044-4

Int. J. Multiphase Flow Vol. 23, No. 1, pp. 25–35, 1997

0301-9322/97 $17.00 + 0.00

HYDRODYNAMIC PROPERTIES OF FRACTALS: APPLICATION OF THE LATTICE BOLTZMANN EQUATION TO TRANSVERSE FLOW PAST AN ARRAY OF FRACTAL OBJECTS

A. ADROVER[1]† and M. GIONA[2]

[1]Dipartimento di Ingegneria Chimica, Università di Roma "La Sapienza", Via Eudossiana 18, 00184 Roma, Italy

[2]Dipartimento di Ingegneria Chimica, Università di Cagliari, Piazza d'Armi, 09123 Cagliari, Italy

(Received 15 December 1994; revised form 12 June 1996)

Abstract—The numerical solution for slow flow past a square array of fractal objects, such as a diffusion limited aggregate (DLA), is addressed by means of the lattice Boltzmann equation (LBE), including a body force term. While the calculated values of the seepage velocity are shown to be independent of the fractal dimension of the objects, the drag force exerted by the fluid is closely linked to fractal dimension. Copyright © 1996 Elsevier Science Ltd.

Key Words: creeping flow, fractal objects, lattice Boltzmann equation, hydrodynamic resistance

1. INTRODUCTION

The theoretical analysis of the creeping flow of a viscous fluid past an array of solid objects is part of the broader study of the relative motion of a mixture of a fluid and solid bodies. In the case of cylindrical objects, both parallel and transverse flows are of mathematical interest since they involve the evaluation of some indeterminate factors and the use of analytic continuation methods around singularities. The literature in the field presents several numerical and analytical approximations for the Stokes equation in the case of a viscous fluid flowing either parallel or perpendicular to the axes of cylinders in square, rectangular, triangular and hexagonal arrays for low and high solid densities (Drummond and Tahir 1984; Sangani and Acrivos 1982(a),(b); Sparrow and Loeffler 1959). For a comprehensive review see Drummond and Tahir (1984).

In each case none of the analytical approaches developed for viscous flow through an array of cylinders can be used if the objects in the elementary cell are 2D fractals (Vicsek 1989; Falconer 1990), due to the complex nature of the boundary conditions to be imposed.

The major purpose of the present article is to determine the hydrodynamic properties of fractal objects, such as a diffusion limited aggregate (DLA) (see Vicsek 1989), in a square array configuration. In particular, we focus on the seepage velocity and on the drag force exerted on the objects by the fluid at low and high solid densities. This problem is addressed by means of the lattice Boltzmann equation.

Lattice gas automata (LGA) (Frisch *et al.* 1987; Wolfram 1986) and the lattice Boltzmann equation (LBE) (McNamara and Zanetti 1988; Higuera and Himenez 1989; Succi *et al.* 1991) have been developed in the last decade as a new method, alternative to direct simulation and to spectral techniques, for solving the partial differential equations of field mechanics and transport (Chen *et al.* 1991; McNamara 1990; Papatzacos 1989; van der Hoef and Frenkel 1991; Balasubramanian *et al.* 1987; Rothman 1988). The ease with which arbitrary complex boundary conditions are handled by the LBE approach (Succi *et al.* 1989; Ginzbourg and Alder 1994) leads us to tackle a great variety of problems related to the physics of disordered and fractal media, e.g. the calculation of transport coefficients and fluid mechanical properties in terms of the microscopic parameters characterizing the structure.

†To whom correspondence should be addressed.

The article is organized as follows. First, we review the fundamental steps in the development of the LBE from the Boolean up to the mean-fluid formulation, also discussing the modification of the collision-propagation microdynamic LBE by means of the introduction of a body force. Then we apply the LBE to the study of transverse viscous flow through a square array of cylinders and compare the LBE results with the Sangani and Acrivos solution and analytical expression for highly diluted and highly concentrated arrays. Finally, we consider transverse viscous flow through a square array of DLA, studying the dependence of the seepage velocity and the drag force on the gyration radius and on the fractal dimension.

2. LGA: FROM MICRODYNAMICS TO THE NAVIER–STOKES EQUATION

Mass and momentum conservation are the local rules governing the dynamics of LGA. These automata can be viewed as a set of pseudo-particles with unit mass and unit speed constrained to move along the links of a regular lattice (Frisch *et al.* 1987; Wolfram 1986).

The automaton state is entirely specified in terms of a set of Boolean variables $n_i(\mathbf{r}, t)$ taking the value one or zero according to whether the $\mathbf{r}$ site holds a particle moving along the ith link or not. A set of collision rules governs momentum transfer between pseudo-particles as in a real fluid. The simultaneous presence of two or more particles with the same speed at the same spatial location is forbidden (exclusion principle). Collisions at each lattice site and the subsequent propagation step define the spatial and temporal evolution of the Boolean field $n_i(\mathbf{r}, t)$ described by means of the microdynamic equation

$$n_i(\mathbf{r} + \mathbf{c}_i, t + 1) = n_i(\mathbf{r}, t) + \Omega_i(n), \qquad [1]$$

where $\mathbf{c}_i$ $(i = 1, \ldots, b)$ is the set of unit vectors connecting a given site of the lattice with its b nearest neighbours, and Ω_i the collision operator, representing the change in the ith occupation number due to collisional interaction.

Because of the mass and momentum conservation rules, the collision term satisfies the following relations:

$$\sum_{i=1}^{b} \Omega_i = 0, \quad \sum_{i=1}^{b} \Omega_i \mathbf{c}_i = 0. \qquad [2]$$

Collisions conserve mass and momentum locally, whereas propagation conserves them globally. As a consequence of the one-speed nature of the automaton, total kinetic energy is automatically conserved, being indistinguishable from mass conservation.

In order to obtain the Navier–Stokes equation, as discussed below, the lattice must be symmetrical enough to ensure isotropy up to at least the fourth order tensor (Frisch *et al.* 1987; Wolfram 1986). This is the case of the hexagonal FHP lattice in two dimensions and of the face-centered hypercubic (FCHC) lattice in four dimensions (used for three-dimensional simulations). Figure 1 shows, for the FHP lattice, one possible set of collision rules conserving mass and momentum and capable of avoiding spurious invariants (Diemer *et al.* 1990).

The spatial and temporal evolution of the automaton can be described by introducing the mean quantities per node N_i, so that the density ρ and mass current $\mathbf{j}$ are defined as

$$N_i(\mathbf{r}, t) = \langle n_i(\mathbf{r}, t) \rangle, \qquad [3]$$

$$\rho(\mathbf{r}, t) = \sum_i N_i(\mathbf{r}, t), \qquad [4]$$

$$\mathbf{j}(\mathbf{r}, t) = \sum_i \mathbf{c}_i N_i(\mathbf{r}, t) = \rho(\mathbf{r}, t)\mathbf{u}(\mathbf{r}, t), \qquad [5]$$

$\mathbf{u}$ being the mean velocity and $\langle \cdot \rangle$ standing for ensemble average.

On a very large lattice, space and time can be regarded as continuous by considering local equilibria varying slowly from point to point. Under the assumption of small Mach numbers, it is possible to use multiscale perturbative analysis to derive from the conservation relations [2] the *macrodynamical* equations, i.e. balance equations for the large-scale and long-term behaviour of

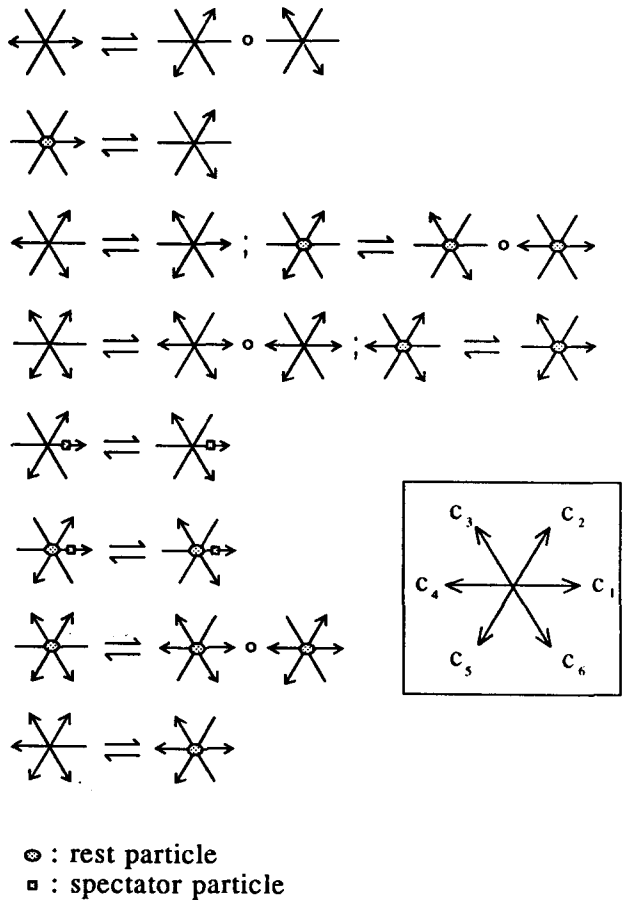

Figure 1. Collision rules of FHP-III nondeterministic model B (Diemer *et al.* 1990).

density and mass currents in the continuum limit. By considering up to second-order terms in velocity and gradients, we obtain (Frisch *et al.* 1987)

$$\partial_t \rho + \mathrm{div}(\rho \mathbf{u}) = 0 \qquad [6]$$

$$\partial_t(\rho u_\alpha) + \partial_\beta(g(\rho)\rho u_\alpha u_\beta) = -\partial_\alpha P(\rho, u) + \partial_\beta(\nu \partial_\beta(\rho u_\alpha)) + \partial_\alpha\left(\frac{D-2}{D}\nu + \zeta\right)\mathrm{div}(\rho \mathbf{u}), \qquad [7]$$

where

$$g(\rho) = \frac{D}{D+2}\,\frac{\rho}{\rho_m}\,\frac{1-2d}{1-d} \qquad [8]$$

$$P(\rho, u) = \frac{\rho_m c^2}{D} - \rho g(\rho)\frac{c_s^2}{c^2}\left(1 + \frac{D}{2} - \frac{c^2}{2c_s^2}\right)u^2. \qquad [9]$$

In [6]–[9], c_s is the speed of sound, ρ_m the density of the moving particles, d the density per link at uniform steady state, and ν and ζ are the kinematic shear and bulk viscosities which depend on the density and on the collision rules adopted (Diemer *et al.* 1990). In [6]–[9], $\partial_t = \partial/\partial t$, $\partial\beta = \partial/\partial x_\beta$, $(\beta = 1, \ldots, D)$ and the Einstein summation convention is adopted.

It can be shown (Frisch *et al.* 1987) that, despite the presence of the factor $g(\rho)$, which is responsible for the non-Galileian invariance of the macrodynamical equation [7], the Navier–Stokes equation for incompressible flow can be recovered exactly by freezing the density at a constant and uniform value ρ_0 everywhere except in the pressure term and rescaling time

$t' \to t/g(\rho_0)$ and viscosity $v' \to vg(\rho_0)$. On the other hand, simulation of compressible flow is still an open question (Qian *et al.* 1992; Qian and Orszag 1993).

3. THE LATTICE BOLTZMANN EQUATION AND BODY-FORCE FORMULATION

In the Boltzmann approach, on the assumption that particles entering into collision have no prior correlation, the occupation numbers n_i in the microdynamical equation [1] are replaced by the corresponding mean population N_i (Higuera and Himenez 1989; McNamara and Zanetti 1988).

By supplementing the averaging procedure with the statistical assumption of molecular chaos, one derives the lattice Boltzmann equation (LBE), which in the linearized version (eliminating rest particles for the sake of simplicity) reads as (Higuera *et al.* 1989, Succi *et al.* 1991)

$$N_i(\mathbf{r} + \mathbf{c}_i, t + 1) = N_i(\mathbf{r}, t) + \sum_j \Phi_{ij}(N_j(\mathbf{r}, t) - N_j^{eq}(\mathbf{r}, t)) + f_i(\mathbf{r}, t), \quad [10]$$

$$\Phi_{ij} = \left.\frac{\partial \Omega(N_i)}{\partial N_i}\right|_{N_i = d} \quad [11]$$

where Φ_{ij} is the linearized collision matrix (evaluated at the zero velocity equilibrium, i.e. linearized around the uniform steady state $N_i = d$) and N_j^{eq} the Fermi–Dirac equilibrium distribution of the mean population N_i (Frisch *et al.* 1987).

The lattice body force $f_i(\mathbf{r}, t)$ is introduced in the LBE for the following reasons. The LBE simulates the Navier–Stokes equations successfully in the case of incompressible flow at low Mach numbers. In this case, the pressure field P, [9], scales linearly with the density of the moving particle ρ_m. This represents an intrinsic constraint in the lattice gas dynamics, equivalent to an equation of state, which limits the possibility of forcing an arbitrary pressure drop without making use of an external body-force term. In LBE simulations, pressure gradients and body forces can be included simply by adding a lattice body force $f_i(\mathbf{r}, t)$ to the microdynamic equation, satisfying the mass conservation rule $\Sigma_i f_i = 0$ (Kadanoff *et al.* 1987; Benzi and Succi 1989). In the case of constant density simulations, the net local body force $\mathbf{f}$ is related to the pressure gradient ∇P and to volume forces $\rho \mathbf{a}$ through the relation

$$\sum_i f_i \mathbf{c}_i = \mathbf{f} = -\nabla P + \rho \mathbf{a}. \quad [12]$$

The body force $\mathbf{f}$ may depend on space and time, may be independent of the velocity (e.g. gravity), may be linear in velocity (e.g. the Coriolis force) or may derive from a generic potential distribution acting on the fluid. In two-dimensional FHP simulations, by further taking into account the different row and column spacing, the relation between the lattice vector f_i and the vector $\mathbf{f} = (f_1, f_2)$ is given by

$$f_i(\mathbf{r}, t) = \frac{1}{4}\left(f_1 - \frac{f_2}{\sqrt{3}}\right) f_i^{(1)} + \frac{f_2}{2\sqrt{3}} f_i^{(2)} \quad [13]$$

where

$$f^{(1)} = \{1, 1, -1, -1, -1, 1\}, \quad f^{(2)} = \{1, 1, 1, -1, -1, -1\} \quad [14]$$

are lattice vectors determining a net momentum transfer in the directions associated with the unit lattice vectors $\mathbf{c}_1$, $\mathbf{c}_2$ (see figure 1).

Let us consider, for example, the flow motion of an incompressible fluid through an $N \times N$ elementary cell in the presence of some solid obstacles and periodic boundary conditions (at the edges of the unit cell).

The implementation of [10] involves three steps for each time instant: the collision step, the propagation step and the reflection step. The latter is introduced to express the boundary conditions. The no-slip boundary conditions at the solid walls are implemented in terms of particle reflection on the solid wall and bouncing back. Let $\mathbf{r}$ be a node in the fluid and $\mathbf{r} + \mathbf{c}_i'$ an adjacent

node belonging to the solid boundary. In the propagation phase, $N_{i'}(\mathbf{r}, t+1)$ moves into $N_{i'}(\mathbf{r}+\mathbf{c}_{i'}, t+1)$. In the reflection step, the mean population $N_{i'}(\mathbf{r}+\mathbf{c}_{i'}, t+1)$ bounces back to the node $\mathbf{r}$ with a reverse velocity $\mathbf{c}_{i''} = -\mathbf{c}_{i'}$, $N_{i''}(\mathbf{r}, t+1) = N_{i'}(\mathbf{r}+\mathbf{c}_{i'}, t+1)$. Because of the reflection condition, the population of sites belonging to the solid boundary are at the end of the entire procedure (collision/propagation/reflection) associated with a single time instant identically equal to zero.

Let N_s be the number of sites occupied by solid bodies. In order to force an arbitrary constant pressure gradient ∇P in the $\mathbf{c}_1$ direction, a constant body force should be applied in each $\mathbf{r}$ fluid site

$$f_i(\mathbf{r}, t) = (-\nabla P/4) f^{(1)}. \qquad [15]$$

From a simple balance equation of forces acting on the fluid, the total drag force F exerted on the solid obstacles can be evaluated and read as

$$F = (-\nabla P) N^2 h^2 \left(1 - \frac{N_s}{N^2}\right), \qquad [16]$$

where h is the unit lattice site size, rescaled so as to take into account the exagonal geometry of each node. However, the detailed knowledge of the pointwise velocity field given by the LBE allows us to estimate to total drag force F also numerically and [16] can be used to check the accuracy of the simulations.

4. TRANSVERSE FLOW THROUGH A SQUARE ARRAY OF CYLINDERS

Exact results for the drag on a cylinder in a periodic array as a function of the volume fraction of the solid are still not available, even for the simple case of creeping flow. Different numerical techniques for solving the governing equations can be found in the literature because of the importance of this configuration in the design of a great deal of heat and mass transfer equipment (Sangani and Acrivos 1982(a)). This problem can easily be addressed by means of the LBE.

Let us consider the transverse steady motion of an incompressible viscous fluid at very low Reynolds numbers through a periodic array of cylinders of radius al, $2l$ being the center-to-center distance between two adjacent cylinders. Let the fluid have a mean velocity U in the y direction (see figure 2) with zero velocity on the cylinder walls and be driven by a pressure gradient $-\nabla P$ in the y direction.

Figure 3 shows the agreement of the LBE simulation results with the two analytical expressions and numerical results (solid line) obtained by Sangani and Acrivos (Sangani and Acrivos 1982(a)). This figure shows the dimensionless quantity $g = 4(-\nabla P)l^2/\mu U$ as a function of the volume fraction $c = \pi a^2/4$. The first analytical expression (dotted curve)

$$g = 8\pi \left[\ln(1/c) - 1.47633597 + \frac{2c - 0.79589781c^2}{1 + 0.48919241c - 1.60486942c^2} \right]^{-1}, \qquad [17]$$

derived by Drummond and Tahir (1984), applies to dilute arrays ($c \ll 1$). The second expression (broken curve) is valid for concentrated arrays. In this case, the application of the usual *lubrication-type* approximation gives

$$g \simeq (9\pi/2\sqrt{2}) \left\{ 1 - \left(\frac{c}{c_{\max}} \right)^{1/2} \right\}^{-5/2}, \quad c_{\max} = \pi/4. \qquad [18]$$

Sangani and Acrivos (Sangani and Acrivos 1982(a)) numerically solved the creeping flow equations of motion by making use of a Taylor series expansion of the stream function and vorticity. The calculated values of $g(c)$ are shown to be in excellent agreement with the corresponding asymptotic expression, [17]–[18] for $c \ll 1$ and for $c \to c_{\max}$ furnishing also an accurate description of the transition range $0.25 < c < 0.4$. In fact, the maximum relative error $\epsilon_{SA} = |g_{SA} - g_{theor}|/g_{theor}$ of the Sangani Acrivos data for low and high concentrated arrays is less than 10^{-3}. In the transition range $0.25 < c < 0.4$, ϵ_{SA} attains the maximum value $\epsilon_{SA} \simeq 4 \times 10^{-2}$ with respect to [17],

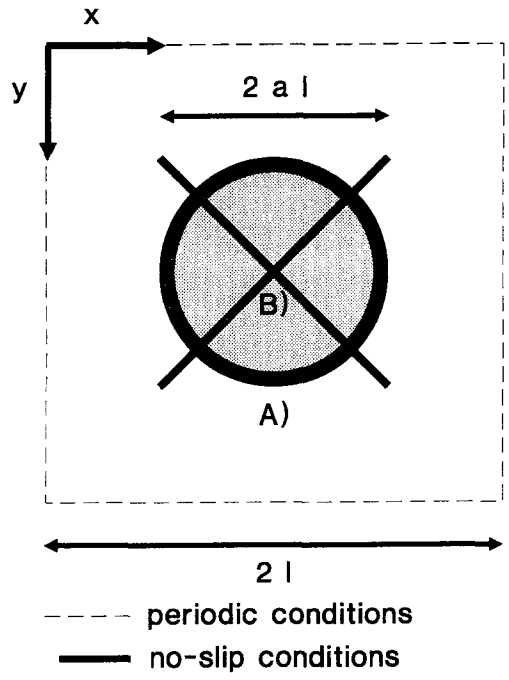

Figure 2. Schematic representation of the 2D-unit square cell used in the simulation of transverse flow around solid objects, including two different objects considered in LBE simulations: (A) cylinder and (B) one-dimensional cross-like object. The objects are located in the middle of the cell. Fluid is forced in the y direction.

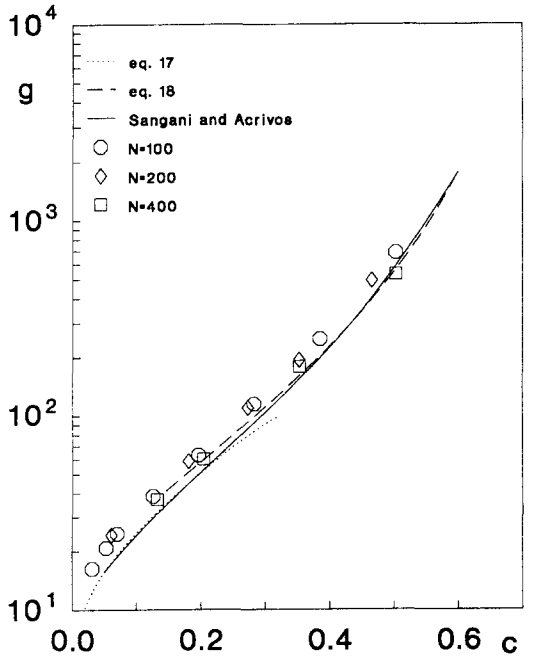

Figure 3. Behaviour of $g = 4(-\nabla P)l^2/\mu U$ vs $c = \pi a^2/4$ for incompressible fluid motion, at low Reynolds numbers, through a square array of cylinders. The points are the results of the LBE simulations on an $N \times N$ elementary cell (see figure 2). The figure shows the Sangani–Acrivos data (solid line) and the analytical results, [17]–[18], valid respectively for dilute and concentrated conditions (dotted lines).

and $\epsilon_{SA} \simeq 6 \times 10^{-2}$ with respect to [18]. Since the analysis of Sangani–Acrivos is valid for all the range of c and is in good agreement with the analytical expressions valid for small and large c, [17]–[18], we will refer to it in order to compare the simulation results obtained by applying the LBE.

LBE simulations were performed on elementary cells of size 100×100, 200×200 and 400×400 lattice units by introducing a body force (to impose a fixed pressure gradient) and choosing non-slip conditions at the cylinder walls and periodic boundary conditions at the edges of the unit cell.

The convergence of the LBE results to the exact solution with the increasing of the lattice size is analysed in figure 4, where the relative error $\epsilon = |g_{LBE} - g_{SA}|/g_{SA}$ between the LBE result g_{LBE} and the Sangani–Acrivos data g_{SA} is plotted vs c for different values of N. It can be observed that for $N = 400$ the percentage error is about 10% over the whole range of c, which can be considered a fairly satisfactory result by further observing that the range of g spans over four decades.

5. TRANSVERSE FLOW THROUGH A SQUARE ARRAY OF FRACTAL OBJECTS

Given the satisfactory results of the numerical check considered above we can go on to study more complex boundary conditions by substituting the cylinder in the elementary cell with a fractal object, specifically a diffusion limited aggregate (DLA) which admits a fractal dimension $D_f \simeq 1.7$ (Vicsek 1989).

The hydrodynamic properties of fractal objects have been addressed by many authors (Meakin *et al.* 1985; Chen *et al.* 1984; Adler 1987, Alder *et al.* 1990). In particular, Adler (Adler 1987) has studied the flow around two-dimensional fractal objects in the zero Reynolds number limit, determining the seepage velocity and the drag force exerted by the fluid on Witten–Sanders (DLA) and cluster–cluster aggregates (Vicsek 1989). Adler claims that the

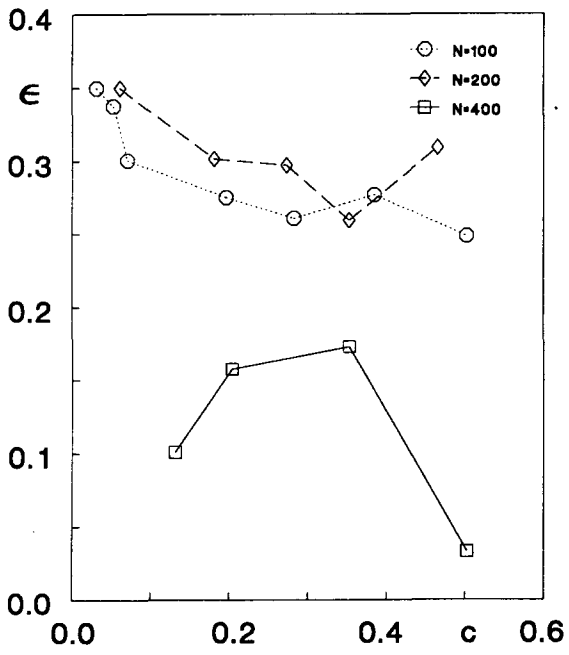

Figure 4. Relative error $\epsilon = |g_{LBE} - g_{SA}|/g_{SA}$ vs c for different values of N for a square array of cylinders. g_{SA} is the value for g obtained by Sangani and Acrivos, g_{LBE} is the result obtained by applying the LBE.

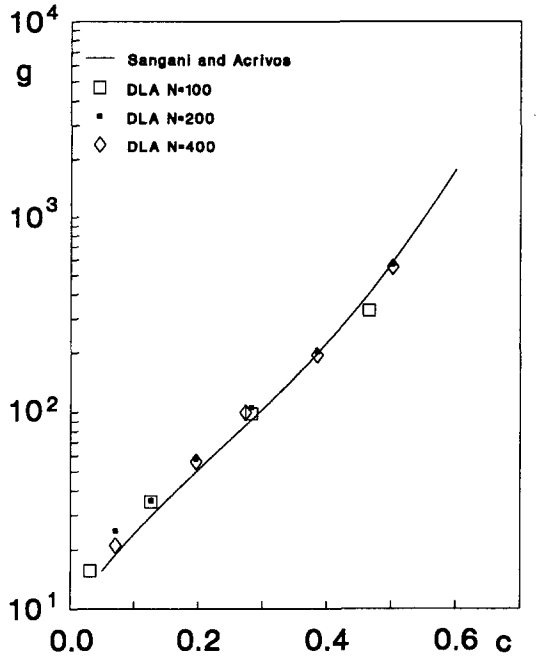

Figure 5. Comparison of the behaviour of $g(c)$ vs c for DLA and Sangani–Acrivos data for cylinders. The simulations were performed on $N \times N$ unit cells.

seepage velocity and the drag force are primarily functions of the gyration radius, while the role of the fractal dimension, if any, is very weak and the average drag is very close to that of circular cylinders.

5.1. Seepage velocity

The LBE simulation results for creeping flow through a square array of DLA are presented in figure 5, which shows the behaviour of g as a function of the dimensionless parameter $c = \pi a^2/4$, al being the radius of the circle in which the considered DLA is inscribed. In practical terms, $2al$ can be viewed as the projection of the fractal object on a plane orthogonal to the fluid motion direction.

The simulation results of figure 5 clearly indicate that, for low Reynolds numbers, a DLA of radius al and the cylinder in which the DLA is inscribed have the same hydrodynamic behaviour, i.e. from a macroscopic point of view, the fluid sets up its motion to the same mean velocity.

This means that two different radially symmetrical objects, having different fractal dimensions but the same projection orthogonal to the flow direction, exhibit the same hydrodynamic resistance to the fluid motion.

This result does not appear to contradict Adler's arguments if it is borne in mind that the ratio between the gyration radius of a cylinder (in 2D) and the gyration radius of a DLA inscribed in the cylinder is very close to unity, in the range of the R_g considered in our simulations (see figure 6). It should also be observed that the largest object considered by Adler has a lattice size of 64 pixels (!), while in our simulations the size of DLA clusters ranges from 500 to 13000 lattice units.

In order to understand whether the linear size al or the gyration radius R_g controls the hydrodynamic resistance, we analyze the incompressible flow in a square array of one-dimensional cross-like objects (see figure 2) for which the ration R_g/al differs significantly from the corresponding ratio for a cylinder or for a DLA (figure 6).

Figure 7 shows the behaviour of g vs c in the case of the cross-like object for different values of N and the comparison with the most accurate LBE results for the square array of cylinders

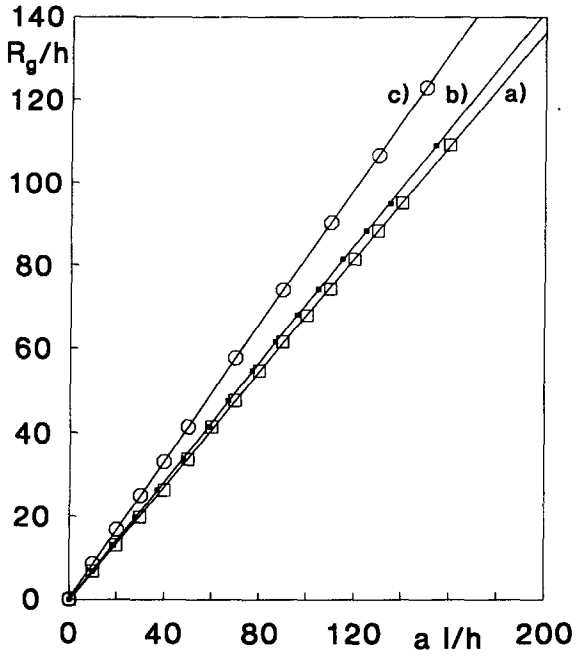

Figure 6. Gyration radius R_g/h vs al/h for different objects: (a) DLA; (b) cylinder; (c) one-dimensional cross-like object (see figure 2). The figure shows the range of al/h considered in the LBE simulations.

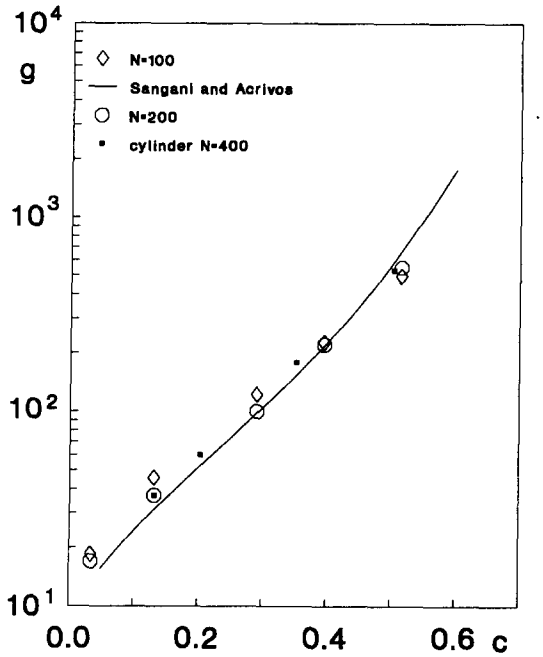

Figure 7. Comparison of the behaviour of $g(c)$ vs c for cross-like object, cylinder ($N = 400$) and the Sangani–Acrivos data for cylinders.

($N = 400$) and with the Sangani–Acrivos curve. As can be noted from figures 3, 5 and 7, for all the structures considered (cylinders, DLA, cross-like objects) the g vs c data practically collapse onto the Sangani–Acrivos curve.

This result enables us to conclude that for two-dimensional flow the fractal dimension is irrelevant to hydrodynamic behaviour at low Reynold numbers and that the linear size controlling hydrodynamic resistance is given by the projection of the object in the direction orthogonal to the fluid motion and not by the gyration radius.

5.2. *Drag force*

We have shown that on applying the same pressure gradient to a fluid flowing through a square array of cylinders and through a square array of DLAs having the same linear dimension al, the fluid sets up its motion to the same mean velocity independently of the fractal dimension of the object.

However, the fractal dimension plays a leading role when the drag force exerted by the fluid is considered.

Under the same fluid dynamical conditions (the same pressure gradient ∇P and the same resulting seepage velocity U) it is possible to compare the total drag force exerted by the fluid on the cylinder F_c and on the DLA, F_D, having the same linear dimension al.

Let N_c and N_D be the numbers of obstacle sites in the elementary cell $N \times N$, belonging respectively, to the cylinder and to the DLA. In terms of the linear dimension al, N_c and N_D read as

$$N_c = \pi\left(\frac{al}{h}\right)^D, \quad N_D = \left(\frac{R_g}{h}\right)^{D_f} = \alpha_D^{D_f}\left(\frac{al}{h}\right)^{D_f}, \qquad [19]$$

where h is the unit lattice site size, $D = 2$, $D_f \simeq 1.7$ the DLA fractal dimension and α_D the prefactor relating the DLA gyration radius R_g to the linear dimension al, ($R_g = \alpha_D al$, $\alpha_D \simeq 0.68$). By applying [16], the ratio F_{D_c} between the total drag force acting on the DLA F_D and on the cylinder F_c

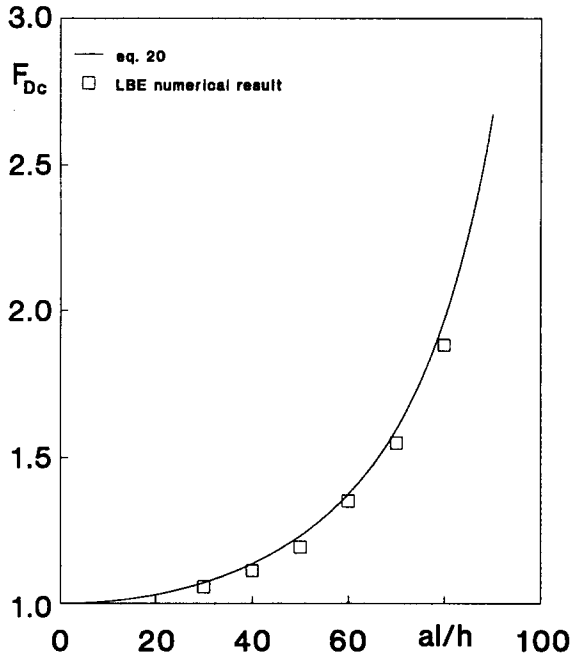

Figure 8. F_{D_c} vs al/h ($N = 200$). The dots represent the LBE numerical results.

attains the form

$$F_{D_c} = \frac{F_D}{F_c} = \frac{N^2 - \alpha_D^{D_f}(al/h)^{D_f}}{N^2 - \pi(al/h)^2}. \qquad [20]$$

Nevertheless, detailed knowledge of the pointwise velocity field of fluid around the object allows us to estimate the drag force exerted on the object itself also numerically. Figure 8 shows the numerical results of F_{D_c} as a function of al/h and the comparison with [20], highlighting the accuracy of the simulations and the validity of [20].

This result contrasts with those of Adler, who claims that the average drag exerted on a fractal object does not depend on its fractal dimension. Figure 8 clearly shows that for small sizes of the DLAs, the ratio F_{D_c} is very close to unity and this can explain the disagreement with the conclusions of Adler, who considers only very small aggregates (made at most by 64 lattice units). In our calculations the fractal aggregates are larger by one to two orders of magnitude. It should be also noticed that in Adler's analysis the fluid is confined between two parallel flat plates. The presence of these plates modifies the streamlines significantly (with respect to our simulations with fully periodic boundary conditions) and limits the hydrodynamic study to low values of the void fraction c.

6. CONCLUSIONS

The LBE is a computational method which easily handles complex boundaries by representing the boundary conditions in terms of particle reflection and bouncing back. In particular, the effect of disorder and fractality on convective-driven phenomena can be properly addressed by means of the LBE including a body-force term.

Detailed knowledge of the pointwise velocity field in the presence of fractal objects allows us to estimate the hydrodynamic radius and the friction factor as a function of geometric parameters characterizing the obstacle structure.

We have shown that, in the case of transverse flow of a viscous fluid through a square array of DLA and through an array of one-dimensional radial symmetric cross-like objects, the corresponding seepage velocity depends on the linear dimension al and does not depend on the fractal dimension, while the total drag force is a function of the fractal dimension. Our analysis

refers to obstacles having fractal dimensions $D_f = 1, 1.7$ and 2 and over the entire range of void fractions c.

For small values of al, the LBE results for the hydrodynamic resistance of fractal aggregates agree with those presented by Adler. As discussed above, this depends on the fact that Adler's analysis is valid only for small c. Deviation from Adler's data, which consider very small clusters and non-periodic boundary conditions, occurs for larger cluster sizes and correspondingly for higher values of c. All the results obtained are valid in the limit of low Reynolds numbers (creeping flow).

Acknowledgements—The authors thank A. Paglianti, M. Schwalm, W. A. Shwalm and A. Viola for useful discussions.

REFERENCES

Adler, P. M. (1987) Hydrodynamic properties of fractal flocs. *Faraday Discuss. Chem. Soc.* **83,** 145–152.

Adler, P. M., Jacquin, C. G. and Quiblier, J. A. (1990) Flow in simulated porous media. *Int. J. Multiphase Flow* **16,** 691–712.

Balasubramanian, K., Hayot, F. and Saam, W. F. (1987) Darcy's law from lattice–gas hydrodynamics. *Phys. Rev.* **A 36,** 2248–2253.

Benzi, R. and Succi, S. (1989) Bifurcation of a lattice gas flow under external forcing. *J. Stat. Phys.* **60,** 69–81,

Chen, S., Diemer, K., Doolen, G. D., Eggert, K., Fu, C., Gutman, S. and Travis, B. J. (1991) Lattice gas automata for flow through porous media. *Physica* D **47,** 72–84.

Chen, Z. Y., Deutch, J. M. and Meakin, P. (1984) Translational friction coefficient of diffusion limited aggregates. *J. Chem. Phys.* **80,** 2982–2983.

Diemer, K., Hunt, K., Chen, S., Shimomura, T. and Doolen, G. (1990) Density and velocity dependence of Reynolds numbers for several lattice gas models. In *Lattice Gas Methods for Partial Differential Equations*, ed. G. Doolen, U. Frisch, B. Hasslacher, S. Orszag, and S. Wolfram, pp. 137–177. Addison-Wesley, Reading, MA.

Drummond, J. E. and Tahir, M. I. (1984) Laminar viscous flow through regular arrays of parallel solid cylinders. *Int. J. Multiphase Flow* **10,** 515–540.

Falconer, K. (1990) *Fractal Geometry: Mathematical Foundation and Application*. J. Wiley and Sons, New York.

Frisch, U., d'Humieres, D., Hasslacher, B., Lallemand, P., Pomeau, Y. and Rivet, Y. P. (1987) Lattice gas hydrodynamics in two and three dimensions. *Complex Systems* **1,** 649–707.

Ginzbourg, I. and Adler, P. M. (1994) Boundary flow condition analysis for the three-dimensional lattice Boltzmann model. *J. Phys. II France A* **4,** 191–214.

Higuera, F. J. and Himenez, J. (1989) Boltzmann approach to lattice gas simulations. *Europhys. Lett.* **9,** 663–668.

Higuera, F. J., Succi, S. and Benzi, R. (1989) Lattice gas dynamics with enhanced collisions, *Europhys. Lett.* **9,** 345–349.

van der Hoef, M. A. and Frenkel, D. (1991) Tagged particle diffusion in 3D lattice gas cellular automata. *Physica D* **347,** 191–197.

Kadanoff, L., McNamara, G. R. and Zanetti, G. (1987) A Poiseuille viscosimeter for lattice–gas automata. *Complex Systems* **1,** 791–803.

McNamara, G. R. (1990) Diffusion in a lattice gas automaton. *Europhys. Lett.* **12,** 329–334.

McNamara, G. R. and Zanetti, G. (1988) Use of the Boltzmann equation to simulate lattice–gas automata. *Phys. Rev. Lett.* **61,** 2332–2335.

Meakin, P., Chen, Z. Y. and Deutch, J. M. (1985) The translational friction coefficient and time dependent cluster size distribution of three dimensional cluster–cluster aggregation. *J. Chem. Phys.* **82,** 3786–3789.

Papatzacos, P. (1989) cellular automata models for fluid flow in porous media. *Complex Systems* **3,** 383–405.

Qian, Y. H., d'Humieres, D. and Lallemand, L. (1992) Lattice BGK models for Navier–Stokes equation, *Europhys. Lett.* **17,** 479–484.

Qian, Y. H. and Orszag, S. A. (1993) Lattice BGK models for the Navier–Stokes equation: nonlinear deviation in compressible regimes, *Europhys. Lett.* **21,** 255–259.

Rothman, H. (1988) Cellular-automation fluids: a model for flow in porous media. *Geophys.* **33,** 509–518.

Sangani, A. S. and Acrivos, A. (1982a) Slow flow past periodic arrays of cylinders with application to heat transfer. *Int. J. Multiphase Flow* **8,** 193–206.

Sangani, A. S. and Acrivos, A. (1982b) Slow flow through a periodic array of spheres. *Int. J. Multiphase Flow* **8,** 343–360.

Sparrow, E. M. and Loeffler, A. L. Jr. (1959) Longitudinal laminar flow between cylinders arranged in regular array. *AIChE J.* **3,** 325–330.

Succi, S., Benzi, R. and Higuera, F. (1991) The lattice Boltzmann equation: a new tool for computational fluid-dynamics. *Physica D* **47,** 219–230.

Succi, S., Foti, E. and Higuera, F. (1989) Three-dimensional flows in complex geometries with lattice Boltzmann method. *Europhys. Lett.* **10,** 433–438.

Vicsek, T. (1989) *Fractal Growth Phenomena*. World Scientific, Singapore.

Wolfram, S. (1986) Cellular automaton fluids 1: basic theory. *J. Stat. Phys.* **45,** 471–526.